AIP | Applied Physics Letters

Ferroelectric BiFeO3 thin-film optical modulators

Minmin Zhu, Zehui Du, Qing Liu, Bensong Chen, Siu Hon Tsang, and Edwin Hang Tong Teo

Citation: Applied Physics Letters **108**, 233502 (2016); doi: 10.1063/1.4953201
View online: http://dx.doi.org/10.1063/1.4953201
View Table of Contents: http://scitation.aip.org/content/aip/journal/apl/108/23?ver=pdfcov
Published by the AIP Publishing

Ferroelectric $BiFeO_3$ thin-film optical modulators

Minmin Zhu,[1,2,3] Zehui Du,[4] Qing Liu,[4] Bensong Chen,[4] Siu Hon Tsang,[4] and Edwin Hang Tong Teo[1,2,3,a)]
[1]*NOVITAS, School of Electrical and Electronic Engineering, Nanyang Technological University, 50 Nanyang Avenue, Singapore 639798*
[2]*CINTRA CNRS/NTU/THALES, UMI 3288 and Research Techno Plaza, 50 Nanyang Drive, Border X Block, Level 6, Singapore 637553*
[3]*Silicon Technologies, Centre of Excellence, 50 Nanyang Avenue, Singapore 639798*
[4]*Temasek Laboratories, Research Techno Plaza, 50 Nanyang Drive, Singapore 637553*

(Received 5 April 2016; accepted 21 May 2016; published online 6 June 2016)

High quality epitaxial $BiFeO_3$ (BFO) thin films have been grown on (001) $SrTiO_3$ substrate by magnetron sputtering. Both *a*-axis and *c*-axis BFO orientations were studied. Prism coupler results reveal that the *c*-axis and *a*-axis refractive indices of the BFO thin films were 2.721 and 2.653 at 632.8 nm; the corresponding propagation losses were 4.3 and 4.6 dB/cm, respectively. An electro-optic (EO) modulator based on such BFO film has been demonstrated with a fast switching time $t = 3.8\ \mu s$ at 632.8 nm for the *a*-axis orientation and $t = 3.4\ \mu s$ for the *c*-axis orientation. Moreover, these BFO films gave the Pockels coefficient $r_{eff} = 19.3$ pm/V for the *c*-axis orientation and $r_{eff} = 15.9$ pm/V for the *a*-axis orientation at 632.8 nm. Such an anisotropic refractive index and linear EO behaviors are attributed to the epitaxial strain and stripe domain structure in the BFO thin films with mixed phases. This study illustrates the suitability of the BFO thin films for EO modulators and optical switches beyond their current extensive spintronic and memory applications. *Published by AIP Publishing*. [http://dx.doi.org/10.1063/1.4953201]

$BiFeO_3$ (BFO) is well known as one important multiferroic material which possesses coupled electric, magnetic, and structural order parameters at room temperature, thereby giving rise to simultaneous ferroelectricity, ferromagnetism, and ferroelasticity.[1,2] As a lead-free material, BFO is regarded as one potential candidate for the next generation of low-power consumable, multifunctional, and environmental-friendly nanoelectronics due to its electric-field controllable interplay of lattice, charge, orbital, and spin degrees of freedom.[3–5] Other than bulk BFO material, the BFO thin film offers a compelling combination of large remnant polarization, high Curie temperature, and strong inherent couplings that have recently attracted enormous attention on spintronic and memory applications which can be addressed both electrically and magnetically.[1,4] Of course, above all, the BFO thin films also demonstrate some interesting optical characteristics such as a small band gap in the visible range (~2.74 eV),[6] weak absorption,[7] large nonlinear optical coefficient,[8] large birefringence,[9,10] and remarkable photovoltaic effect.[11,12]

The well-established electro-optic (EO) modulator is indispensable in the modern telecommunications industry. Standard EO modulators are based on microscope ferroelectric $LiNbO_3$ (LNO) with an efficient Pockels coefficient of ~30 pm/V.[13] Although the conventional lead-based ferroelectrics such Pb(Zr,Ti)O_3 (PZT),[14,15] (Pb,La)(Zr,Ti)O_3 (PLZT),[16] and $Pb(Mg_{1/3},Nb_{2/3})O_3$-$PbTiO_3$ (PMN-PT)[17] have also been used as the modulating media due to their high transparency (~80%) and large Pockels coefficient (100–270 pm/V), the pollution to the environment cannot be ignored as a result of the existence of lead. Recently, there have been extensive effects to create lead-free $BaTiO_3$ (BTO) and their derivatives.[18,19] However, the ferroelectric transition of the BTO thin film is just above room temperature, which seriously limited its operation over wide temperature ranges. By constant, ferroelectric transition temperature of BFO is around 830 °C which is much higher than room temperature, maybe offer promise for thin-film optical modulator operating over a wide temperature range. Meanwhile, first principle calculations reveal that a fully tetragonal phase with huge $c/a = \sim 1.26$ and a very giant polarization of ~150 $\mu C/cm^2$ can be obtained at a highly compressive strained BFO thin films.[5,20,21] Moreover, the BFO thin film also possesses a mixed tetragonal-monoclinic-rhombohedral transition phase induced by the epitaxial stress,[21–23] thereby leading to the presence of morphotropic phase boundary (MPB) which is similar to a rhombohedral-to-tetragonal phase boundary in the conventional lead-based PZT and PMN-PT thin films. Therefore, the lead-free BFO films possess the potential of optical modulators as a substitute for the lead-based materials such as PZT, PLZT, and PMN-PT. In this letter, we fabricated the thin-film optical modulators based on high-quality epitaxial BFO thin films along the *a*-axis and *c*-axis orientation. Their refractive indices, propagation loss, switching time, and Pockels coefficients for both *c*-axis and *c*-axis orientations were also studied systematically.

Single crystal (001) $SrTiO_3$ (STO) was ultrasonically cleaned in acetone, isopropyl alcohol, and de-ionized water subsequently. $BiFeO_3$ ceramic disk with 10% bismuth excess was used to deposit the BFO thin films on STO substrates by magnetron sputtering. The films deposited at a substrate temperature of ~300 °C and at a pressure of ~5 mTorr by using mixed oxygen and argon gases. The films were post-annealed by rapid thermal processing (RTP) under oxygen atmosphere at 700 °C for 20 min for high crystallinity. X-ray diffraction

a)Author to whom correspondence should be addressed. Electronic mail: htteo@ntu.edu.sg

(XRD, Shimadzu), prism coupler spectroscopy (Metricon), and transmission electron microscopy (TEM, JEOL2010F) were performed to investigate the samples. An experimental optical setup using a 632.8 nm He–Ne laser with transmission geometry was built to study the *a*-axis and *c*-axis electro-optic effects of the BFO thin films.

Fig. 1(a) shows a typical θ-2θ XRD pattern of BFO thin film grown on (001) STO substrate. Only the (oo*l*) peaks from the film and the substrate are evident, indicating that the as-grown BFO thin films are epitaxially grown on the substrates. The full width at half maximum (FWHM) of the rocking curve for the (002) BFO reflection is ~0.39° (not shown), which is relatively narrow and confirms the high crystalline quality of the samples. Previous studies have shown that the BFO thin films grown on (001) or (101) STO substrates are monoclinically distorted from the rhombohedral structure due to the epitaxial constraint.[24,25] From these diffraction angles, the d spacing of (001) BFO films is determined to be 4.02 Å, larger than that of bulk BFO (~3.96 Å). This indicates an elongation of out-of-plane lattice dimension, which is a result of the in-plane compression from STO substrate. Fig. 1(b) shows the corresponding Φ scans for such (001)-oriented BFO thin film and STO substrate. It is worthwhile to note that the Φ scan of the (001) BFO peak clearly has four sharp peaks separated by 90°, which is also consistent with the monoclinic structure. To further understand the crystal structure of the BFO films, a high resolution TEM was used to study the cross-section interface between the BFO film and the STO substrate. Fig. 1(c) reveals a representative cross-sectional TEM image of the BFO film on the STO substrate. It can be seen that the BFO thin film is of high crystallinity. As shown in the inset of Fig. 1(c), the selected area diffraction (SAED) pattern of the BFO thin films derived from fast Fourier transform (FFT) further confirms the single crystalline quality of the films. Fig. 1(d) demonstrates the schematic for crystal structure of monoclinic BFO film on cubic STO substrate, as well as the corresponding HRTEM image of the interface between the film and the substrate. It is noted that the interplanar spacing of the monoclinic BFO films are calculated to be $d_{\langle 200\rangle} = 2.846$ Å and $d_{\langle 020\rangle} = 2.776$ Å, respectively. According to TEM and XRD analyses, the as-grown BFO film on the (001) STO substrate is monoclinic phase with $a = 5.692$ and $b = 5.532$, which is in agreement with values typically reported for this phase by magnetron sputtering.[25,26] In addition, we also observe the coexisting of the monoclinic and tetragonal mixed phases, as shown in Fig. 1(e). It is believed that the rhombohedral-tetragonal-monoclinic transition strongly depends on the thickness and growth conditions.[22,26] Plenty of study have confirmed that such MPB-like interfaces in BFO films can effectively enhance the electric properties of the BFO thin film. For example, the longitudinal piezoelectric coefficient can reach 120 pm/V in the mixed-phase BFO film compared with 65 pm/V in the pure-R phase and 30 pm/V in the pure-T phase.[27] Therefore, it is expect that such mixed phase boundary in BFO thin film can improve its optical and electro-optic properties.

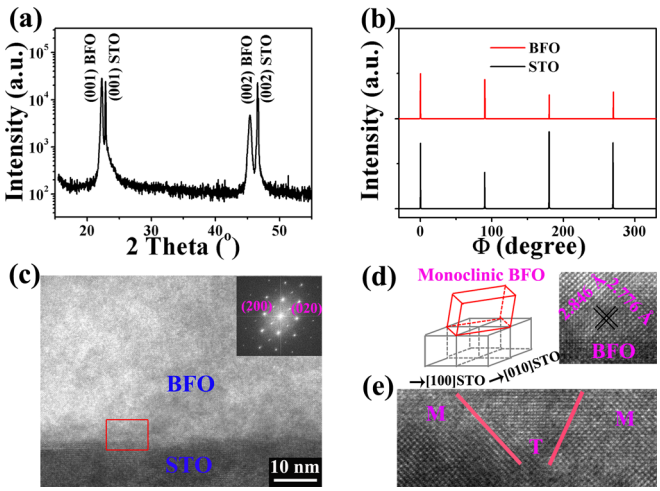

FIG. 1. (a) Typical θ-2θ XRD scans of BFO thin films grown on (001) STO substrate. (b) Φ scans for (001)-oriented thin films. (c) Low-magnification cross-section TEM image of the samples. The inset is the FFT of the BFO film area. (d) Schematic for crystal structure of epitaxial monoclinic BFO thin films grown on cubic STO substrate, as well as the interplanar spacing of the BFO films. (e) High resolution TEM image of the phase boundaries between M and T regions, indicated by redline.

Fig. 2 shows the TE (transverse electric, *c*-axis) and TM (transverse magnetic, *c*-axis) guided-mode spectra for the as-grown BFO thin films. Three TE and three TM modes have been excited. The sharp reflectivity dips indicate a good confinement of light into the waveguide layer of the films. Using all the TE and TM modes in the spectra, the refractive indices of the BFO films can be determined to be $n_{TE} = 2.721$ and $n_{TM} = 2.653$, giving a refractive-index difference

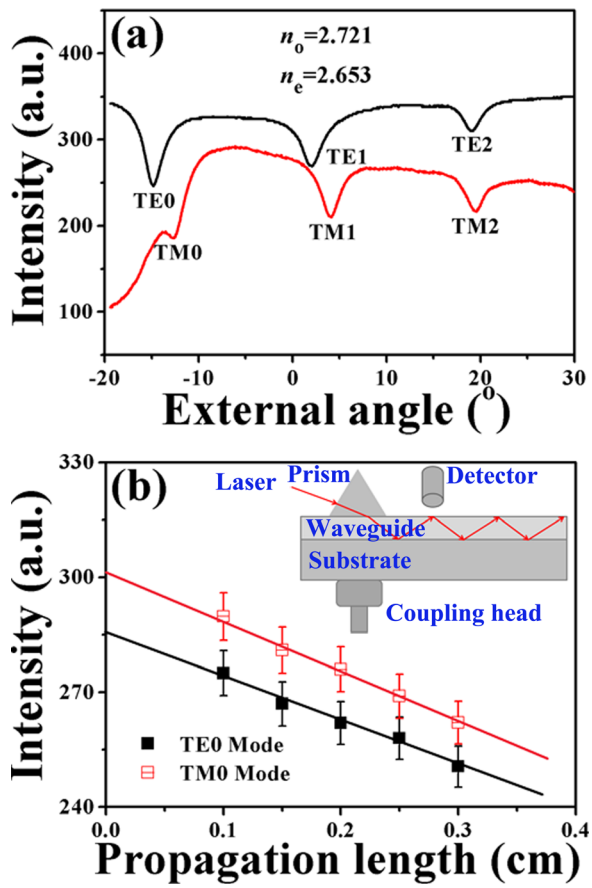

FIG. 2. (a) TE and TM mode spectra at a wavelength of 632.8 nm for the BFO thin films grown on (001) STO substrate. (b) Scattered intensity from TE0 and TM0 modes of the BFO films at 632.8 nm. The inset is a schematic diagram of experimental arrangement for surface scattering loss.

(birefringence), i.e., $\Delta n = n_{TE} - n_{TM} = 0.068$ at $\lambda = 632.8$ nm. The large birefringence can be ascribed to the highly (001)-oriented texture of the BFO film. The refractive indices of the samples are also in agreement with the values of the epitaxial BFO thin films prepared by molecular beam epitaxy and pulse laser deposition.[9] Noted that the surface scattering is the main propagation loss in transparent ferroelectric thin films which can be derived for the film from measurements of the out-of-plane scattered light intensity. Fig. 2(b) shows the scattered intensity form TE0 and TM0 modes at 632.8 nm. A least square fit gives the propagation losses of 4.3 dB/cm and 4.6 dB/cm for TE0 and TM0 modes at 632.8 nm, respectively. Although the accuracy of propagation loss is limited due to the small samples size and the short scattering length, the prism coupler gives a good approximation, and the results are comparable to those values in other perovskite ferroelectric thin films such as PZT and PMN-PT.[14,28] Obviously, the prism coupling technique is really one quick and easy method to determine the refractive index and propagation loss of the transparent ferroelectric thin films, as compared to spectroscopic ellipsometry which always requires substantial effort to simulate the raw data and hence extract mathematically for the tensor components along the ordinary and extraordinary principal axes of BFO thin films.[9] Table I summarizes the derived values of the ordinary (n_o) and extraordinary (n_e) refractive indices for perovskite EO materials using the prism coupling method at room temperature, as well as the corresponding propagation loss. These perovskite ferroelectric materials are divided into two categories: lead-based EO materials (PZT,[14] PLZT,[16] (Pb,La)TiO_3 (PLT),[29] and PMN-PT[28]) and lead-free EO materials (LNO,[30] BTO,[31] (Ba,Sr)TiO_3 (BST),[32] and $Na_{0.5}K_{0.5}NbO_3$ (KNN)[33]). Obviously, the BFO thin film demonstrates the largest refractive index of ~2.721 at 632.8 nm which is propitious to utilize the prism coupler, compared to other perovskite EO materials. Moreover, the BFO thin film also possesses a low propagation loss which can be further reduced by optimizing the growth process. Such a large refractive index and a low propagation loss demonstrate the potential of BFO as a substitute for the lead-based materials in optical modulators.

An experimental optical setup with transmission geometry was used to carry out the electro-optic measurement of the BFO thin films, as shown in Fig. 3(a). The details of this method were presented in our previous works.[15,34] In order

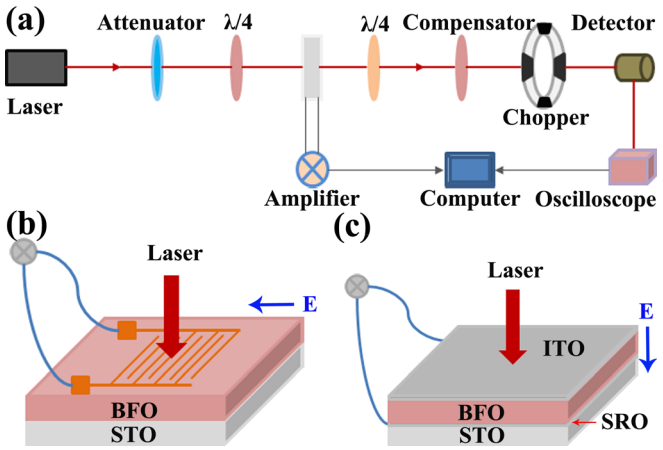

FIG. 3. (a) Schematic diagram of optical setup for electro-optic measurement in BFO thin films. (b) Interdigital electrodes with 100 nm Au and 5 nm Ti are used in the *a*-axis orientation. (c) ITO and $SrRuO_3$ thin films are used the top and bottom electrodes in the *c*-axis orientation.

to determine the *a*-axis and *c*-axis electro-optic properties of the BFO thin films, the electric fields along the two different orientations are developed, as shown in Figs. 3(b) and 3(c). In the typical transmission geometry, an input laser beam is focused through the film onto the top electrode. Under the applied electric field (*a*-axis, parallel to film surface), the laser beam propagates through the BFO thin film (Fig. 3(b)). Then, an oscilloscope converts this phase shift into an intensity modulation, which is measured by a photodetector locked to the frequency of the excitation voltage. On the other hand, the second electric field direction is perpendicular to the surface (*c*-axis), as shown in Fig. 3(c). Transparent indium tin oxide (ITO) and $SrRuO_3$ (SRO) thin film are deposited as the top and bottom electrodes, respectively.

Fig. 4(a) shows a strong field-induced optical modulation, as the external electric field is varied from 20 to 60 kV/cm. The field-induced refractive index changes have been summarized as functions of the external electric field (E), as shown in Fig. 4(b). It is noted that all the BFO thin films exhibit linear EO behavior and a strong dependence of EO responses on the electric field orientation is clearly seen. The linear EO coefficient (Pockels effect) of the BFO thin films is given by[15]

$$\Delta n = -\frac{1}{2} n^3 r_{\text{eff}} E, \tag{1}$$

TABLE I. Derived values of the ordinary (n_o) and extraordinary (n_e) refractive indices for perovskite EO materials using prism coupling method at room temperature.

Materials	n_o	n_e	Propagation loss (dB/cm)	Wavelength (nm)	References
BFO	2.721	2.653	4.3–4.6	632.8	This work
PZT	2.454	2.433	~4.2	632.8	14
PLZT	2.365	2.345	~4.0	632.8	16
PLT	2.375	2.271	…	633	29
PMN-PT	2.542	2.448	4.1–4.8	633	28
LNO	2.233	2.203	…	632.8	30
BTO	2.224	2.219	…	1539	31
BST	2.219	2.170	2.6–3.0	632.8	32
KNN	2.286	2.232	…	655	33

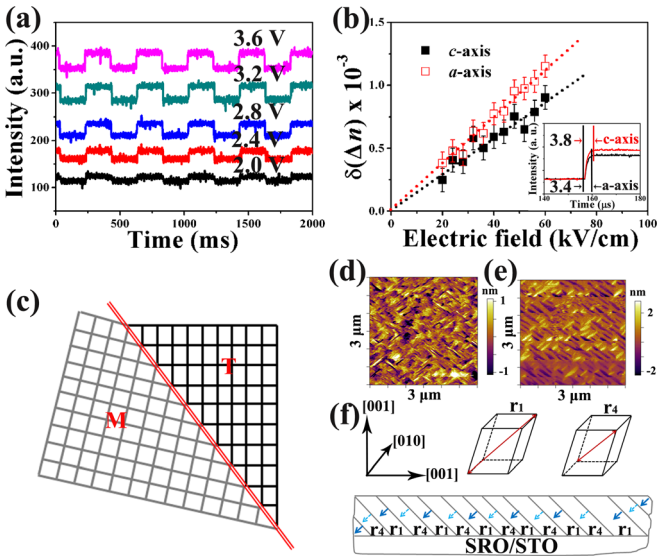

FIG. 4. (a) The electrical-induced optical modulation by BFO thin film under the applied electric fields. (b) Linear *a*-axis and *c*-axis EO properties of the BFO films as functions of the electric field (E). The insets are the corresponding switching times for the *a*-axis and *c*-axis orientation. (c) Schematic illustration of the strain gradient of the interface (red line) between the M and T phases. (d) Topography and (e) PFM image (3 μm × 3 μm) of BFO thin films on miscut STO substrate. (f) Schematic drawings of two domains in the BFO films on the STO substrate.

where n and E are the refractive index and the applied electric field, respectively. In this case, the *a*-axis and *c*-axis coefficients of the BFO thin films were calculated to be 19.3 and 15.9 pm/V, respectively. This value is superior to 12.0 ± 0.3 pm/V of (101)-oriented BFO thin film by pulsed laser deposition (PLD) method.[9] As shown in the inset of Fig. 4(b), the EO modulator based on such BFO films has been demonstrated with a fast switching time $t = 3.8\ \mu$s at 632.8 nm for the *a*-axis samples and $t = 3.4\ \mu$s for the *c*-axis samples, which is comparable to those values typically reported in PMN-PT thin films.[35] In fact, the linear EO coefficient of perovskite ferroelectrics strongly depends on the spontaneous polarization and dielectric constant[36]

$$r_{ijk} = 2\varepsilon_0(\varepsilon_{kl} - \delta_{kl})g^o_{eff,ijk}\frac{P_s}{\xi^3}, \tag{2}$$

where r_{ijk}, ε_0, ε_{kl}, δ_{kl}, $g^o_{eff,ijk}$, P_s, and ξ are the linear EO coefficient, dielectric permittivity, dielectric tensor, Kronecker delta, temperature independent quadratic polarization-optic coefficient of the octahedral, spontaneous polarization, and packing density of octahedral ($\xi = 1$ for perovskite materials). It can be seen that the linear EO coefficient of perovskite ferroelectric thin film is proportional to its spontaneous polarization (P_s) which significantly lies on the epitaxial strain and domain structure in BFO thin films.[24] The strain-driven MPB of BFO films on STO substrate has been extensively discussed previously.[26,37] It can be considered as the free-energy crossover between the giant axial T-like phase and the R-like phase akin to the bulk during the relaxation process of the elastic energy.[37,38] In the mixed-phase BFO system, the formation of dislocation is replaced by the formation of the M-like phase, as shown as Fig. 4(c). To accommodate the lattice mismatch between T and M phases, the more compliant M phase exhibits an expansion of the out-of-plane lattice constant whereas the strain relaxes with the distance apart from the phase boundary. A similar strain relaxation trend can be found in lanthanum-doping tetragonal-like BFO thin films.[38] Such a strain gradient should account for the extraordinary polarization in the mixed-phase BFO films.[27] Figs. 4(d) and 4(e) show the topography and piezoelectric force microscopy (PFM) images of the BFO thin films. The BFO films grown (001) STO substrate demonstrate a typical twin-wall orientations for stripe-like domains which match well with those predicted from phase-field simulation.[39] It is known that different domain structures of the BFO films grown on miscut (001) STO substrates result in different ferroelectric properties.[40] The in-plane PFM images confirm two variants (r_1 and r_4) in the BFO film on miscut STO substrates (Fig. 4(e)), which correspond to 71° and 109° domains.[41] In this case, the elastic strain energy in BFO films are effectively relieved without forming additional domain variants (r2 and r3).[38,40] As a result, the epitaxial strains and stripe domain structure in the mixed-phase BFO thin film should be responsible for its anisotropic optical and EO behaviors.[15]

In summary, the electro-optic modulator based high quality epitaxial (001)-oriented BFO thin films has been demonstrated. Both *a*-axis and *c*-axis BFO orientations were studied. The *c*-axis and *a*-axis refractive indices of BFO thin films were 2.721 and 2.653 at 632.8 nm; the corresponding propagation losses were 4.3 and 4.6 dB/cm, respectively. These thin-film BFO modulators have also been demonstrated with a fast switching time $t = 3.8\ \mu$s at 632.8 nm for the *a*-axis orientation and $t = 3.4\ \mu$s for the *c*-axis orientation. Moreover, it gave a large Pockels coefficient $r_{\text{eff}} = 19.3$ pm/V for the *c*-axis film and $r_{\text{eff}} = 15.9$ pm/V for the *a*-axis films at 632.8 nm. Besides the nature of electricity and magnetism, this study illustrates the potential of the BFO thin films for optoelectronic applications such as electro-optic modulators and optical switches beyond their spintronic and memory applications.

The authors would like to acknowledge the funding support from NTU-A*STAR Silicon Technologies Centre of Excellence under the program Grant (No. 1123510003) and Singapore Ministry of Education Academic Research Fund (Tier 2 No. MOE2013-T2-2-050).

[1]J. Wang, J. B. Neaton, H. Zheng, V. Nagarajan, S. B. Ogale, B. Liu, D. Viehland, V. Vaithyanathan, D. G. Schlom, U. V. Waghmare, N. A. Spaldin, K. M. Rabe, M. Wuttig, and R. Ramesh, Science **299**, 1719 (2003).
[2]J. C. Yang, Q. He, P. Yu, and Y. H. Chu, Annu. Rev. Mater. Res. **45**, 249 (2015).
[3]T. Zhao, A. Scholl, F. Zavaliche, K. Lee, M. Barry, A. Doran, M. P. Cruze, Y. H. Chu, C. Ederer, N. A. Spaldin, R. R. Das, D. M. Kim, S. H. Baek, C. B. Eom, and R. Ramesh, Nat. Mater. **5**, 823 (2006).
[4]G. Catalan and J. F. Scott, Adv. Mater. **21**, 2463 (2009).
[5]R. J. Zeches, M. D. Rossell, J. X. Zhang, A. J. Hatt, C.-H. Yang, A. Kumar, C. H. Wang, A. Melville, C. Adamo, G. Sheng, Y.-H. Yang, J. F. Ihlefeld, R. Erni, C. Ederer, V. Gopalan, L. Q. Chen, D. G. Schlom, N. A. Spaldin, L. W. Martin, and R. Ramesh, Science **326**, 977 (2009).
[6]J. F. Ihlefed, N. J. Podraza, Z. K. Liu, R. C. Rai, X. Xu, T. Heeg, Y. B. Chen, J. Li, R. W. Collines, J. L. Musfeldt, X. Q. Pan, J. Schubert, R. Ramesh, and D. G. Schlom, Appl. Phys. Lett. **92**, 142908 (2008).
[7]H. F. Dong, Z. G. Wu, S. Y. Wang, W. H. Duan, and J. B. Li, Appl. Phys. Lett. **102**, 072905 (2013).
[8]R. C. Haislmaier, N. J. Podraza, S. Denev, A. Melville, D. G. Schlom, and V. Gopalan, Appl. Phys. Lett. **103**, 031906 (2013).

[9]D. Sando, P. Hermet, J. Allibe, J. Bourderionnet, S. Fusil, C. Carrétéro, E. Jacquet, J. C. Mage, D. Dolfi, A. Barthélémy, Ph. Ghosez, and M. Bibes, Phys. Rev. B **89**, 195106 (2014).
[10]J. P. Rivera and H. Schmid, Ferroelectrics **204**, 23 (1997).
[11]T. Choi, S. Lee, Y. J. Choi, V. Kiryukhin, and S. W. Cheong, Science **324**, 63 (2009).
[12]R. Guo, L. You, Y. Zhou, Z. S. Lim, Y. Peng, and J. L. Wang, Nat. Commun. **4**, 1990 (2013).
[13]C. L. Sones, P. Ganguly, Y. J. Ying, F. Johann, E. Soergel, R. W. Eason, and S. Mailis, Opt. Express **17**, 23755 (2009).
[14]M. M. Zhu, Z. H. Du, and J. Ma, J. Appl. Phys. **106**, 023113 (2009).
[15]M. M. Zhu, Z. H. Du, L. Jing, A. I. Y. Tok, and E. H. T. Edwin, Appl. Phys. Lett. **107**, 031907 (2015).
[16]Z. H. Du, T. S. Zhang, M. M. Zhu, and J. Ma, J. Appl. Phys. **105**, 061612 (2009).
[17]X. M. Wan, H. S. Luo, X. Y. Zhao, D. Y. Wang, H. L. W. Chan, and C. L. Choy, Appl. Phys. Lett. **85**, 5233 (2004).
[18]C. Xiong, W. H. P. Pernice, J. H. Ngai, J. W. Reiner, D. Kumah, F. J. Walker, C. H. Ahn, and H. X. Tang, Nano Lett. **14**, 1419 (2014).
[19]D. Y. Wang, S. Li, H. L. W. Chan, and C. L. Choy, Appl. Phys. Lett. **96**, 061905 (2010).
[20]D. Ricinschi, K. Y. Yun, and M. Okuyama, J. Phys.: Condens. Matter **18**(6), L97 (2006).
[21]D. Mazumdar, V. Shelke, M. Iliev, S. Jesse, A. Kumar, S. V. Kalinin, A. P. Baddorf, and A. Gupta, Nano Lett. **10**, 2555 (2010).
[22]Z. Fu, Z. G. Yin, N. F. Chen, X. W. Zhang, Y. J. Zhao, Y. M. Bai, Y. Chen, H. H. Wang, X. L. Zhang, and J. L. Wu, Appl. Phys. Lett. **104**, 052908 (2014).
[23]Y. J. Qi, C. W. Huang, Z. H. Chen, Z. L. Luo, Y. Q. Wang, J. Guo, T. White, J. L. Wang, C. Gao, T. Sritharan, and L. Chen, Appl. Phys. Lett. **99**, 132905 (2011).
[24]J. F. Li, J. L. Wang, M. Wuttig, R. Ramesh, N. Wang, B. Ruette, A. P. Pyatakov, A. K. Zvezdin, and D. Viehland, Appl. Phys. Lett. **84**, 5261 (2004).
[25]D. Kan and I. Takeuchi, J. Appl. Phys. **108**, 014104 (2010).
[26]H. J. Liu, P. Yang, K. Yao, and J. Wang, Appl. Phys. Lett. **98**, 102902 (2011).
[27]J. X. Zhang, B. Xiang, Q. He, J. Seidel, R. J. Zeches, P. Yu, S. Y. Yang, C. H. Wang, Y. H. Chu, L. W. Martin, A. M. Minor, and R. Ramesh, Nat. Nanotechnol. **6**, 98 (2011).
[28]Y. L. Lu, G. H. Jin, M. C. Golomb, S. W. Liu, H. Jiang, F. L. Wang, J. Zhao, S. Q. Wang, and A. J. Drehman, Appl. Phys. Lett. **72**, 2927 (1998).
[29]A. Boudrioua, J. C. Loulergue, E. Dogheche, and D. Remiens, J. Appl. Phys. **85**, 1780 (1999).
[30]S. Fries and S. Bauschulte, Phys. Status Solidi **125**, 369 (1991).
[31]F. Leroy, A. Rousseau, S. Payan, E. Dogheche, D. Jenkins, D. Decoster, and M. Maglione, Opt. Lett. **38**, 1037 (2013).
[32]D. Y. Wang, H. L. W. Chan, and C. L. Choy, Appl. Opt. **45**, 1972 (2006).
[33]S. I. Khartsev, M. A. Grishin, and A. M. Grishin, Appl. Phys. Lett. **86**, 062901 (2005).
[34]M. M. Zhu, J. Wu, Z. H. Du, R. Y. J. Tay, H. L. Li, B. Özyilmaz, and E. H. T. Teo, Nanoscale **7**, 14730 (2015).
[35]M. M. Zhu, X. L. Chen, Z. H. Du, and J. Ma, AIP Adv. **1**, 042163 (2011).
[36]P. Gunter, *Electro-Optic and Photo-Reflective Materials* (Springer-Verlag, New York, 1991).
[37]H. J. Liu, P. Yang, K. Yao, K. P. Ong, and J. Wang, Adv. Funct. Mater. **22**, 937 (2012).
[38]L. You, P. Caesario, L. Fang, P. Ren, L. Wang, Y. Zhou, A. Gruverman, and J. L. Wan, Phys. Rev. B **90**, 134110 (2014).
[39]Y. H. Chu, M. P. Cruz, C. H. Yang, L. W. Martin, P. L. Yang, J. X. Zhang, K. Lee, P. Yu, L. Q. Chen, and R. Ramesh, Adv. Mater. **19**, 2662 (2007).
[40]H. W. Jang, D. Ortiz, S. H. Baek, C. M. Folkman, R. R. Das, P. Shafer, Y. B. Chen, C. T. Nelson, X. Q. Pan, R. Ramesh, and C. B. Eom, Adv. Mater. **21**, 817 (2009).
[41]Y. B. Chen, M. B. Katz, X. Q. Pan, R. R. Das, D. M. Kim, S. H. Baek, and C. B. Eom, Appl. Phys. Lett. **90**, 072907 (2007).